Dynamics of vitreous Ag-Ge-Se

R. J. Dejus,* D. J. LePoire, S. Susman, K. J. Volin, and D. L. Price
Materials Science Division and Intense Pulsed Neutron Source, Argonne National Laboratory, Argonne, Illinois 60439-4843
(Received 12 March 1991; revised manuscript received 18 July 1991)

The dynamic scattering function $S(Q,E)$ for vitreous g-$Ag_4Ge_3Se_9$ at $T=15$ K has been measured by time-of-flight inelastic neutron scattering using an incident energy of ~ 60 meV. The neutron measurements have been complemented by room-temperature Raman-scattering measurements. The data are presented and discussed in terms of the elastic structure factor $S_{el}(Q)$, the total structure factor $S(Q)$, the neutron-weighted generalized one-phonon vibrational density of states (GVDOS), and the Q dependence of the dynamic structure factor $S(Q,E)$ at selected energy excitations. Comparisons are made with experimental results for pure $GeSe_2$ glass, and with calculations based on the method of normal-mode analysis to interpret the data. The introduction of Ag into the Ge-Se glassy network has a profound effect on the vibrational spectrum and the intermediate-range order. The $GeSe_{4/2}$ tetrahedron, however, generally accepted as the local structural element of pure $GeSe_2$ glass, remains a valid structural component also in the heavily Ag-doped glass. We find that the so-called companion line in the Raman spectrum for g-$GeSe_2$ disappears upon doping with Ag, indicating a change of the intermediate-range order. Moreover, there is a large increase in the population of vibrational modes below ~ 200 cm^{-1} in both the GVDOS and the Raman spectrum. These modes can be associated with vibrational modes of Ag atoms interacting with three Se in a nearly planar pyramidal arrangement. We derive 30 kdyn/cm for the Ag-Se stretching constant.

I. INTRODUCTION

The study of network dynamics by inelastic neutron scattering and spectroscopic techniques is important for determining the short- and intermediate-range orders in noncrystalline solids. Combined with information from direct structural probes, such as x-ray and neutron diffraction and computer modeling methods, it yields a coherent picture of the network structure.[1]

The chalcogenide glass $GeSe_2$ provides an excellent example where all these methods have been applied[2-6] and where the short-range order has been determined to a high degree of confidence. The stoichiometric $GeSe_2$ glass consists locally of $GeSe_{4/2}$ tetrahedra interconnected mainly through corner sharing but also through edge sharing—30–40 % are edge-shared tetrahedra according to Refs. 3 and 6. The glass also exhibits intermediate-range order as manifested in the appearance of the pronounced first sharp diffraction peak (FSDP) in the structure factor $S(Q)$, whose origin has given rise to many speculations.[7] Suggestions have been made, for example, that sections of two-dimensional layers[8] consisting of both corner-shared and edge-shared $GeSe_2$ tetrahedra (a remnant from the crystalline phase) with a correlation length of the order of 20 Å are creating the FSDP. However, the FSDP is observed in a variety of chalcogenide and oxide glasses[9] exhibiting dimensionalities ranging from zero (molecular glasses such as P-Se) to three (vitreous SiO_2), and it is even observed in the liquid state. There is no generally accepted explanation for the FSDP at this moment.

The Ge-Se glass alloyed with Ag has very important practical applications and the purpose of the present work is to study the effect on vibrational and structural properties of the Ge-Se network upon doping with Ag. This paper reports the effect of Ag doping on the dynamical properties as measured by inelastic neutron scattering and by Raman scattering, and its implications concerning the short- and intermediate-range orders. The structure of vitreous Ag-Ge-Se, derived from high-resolution radial distribution functions using the method of pulsed neutron diffraction, is planned to be presented elsewhere.[10] The glass-forming region for the ternary Ag-Ge-Se system and the preparation technique are discussed in Ref. 10. The composition of the glass studied here and in Ref. 10 is $Ag_4Ge_3Se_9$ which also may be written as $(Ag_2Se)_2(GeSe_2)_3Se$ or $Ag_4(GeSe_3)_3$ to emphasize its relationship to either g-$GeSe_2$ or g-$GeSe_3$. The composition is on the Se-rich side of the Ag_2Se-$GeSe_2$ tie line, as was found necessary in order to form a homogeneous glass when quenching from the melt.

The formalism for analysis of inelastic-neutron-scattering data from amorphous materials has been reported in the preceding papers on vitreous silica[11] and $GeSe_2$ glass[4] and will not be reproduced here, apart from some relationships important for understanding the analyses.

II. SAMPLE PREPARATIONS

The vitreous sample was synthesized from high-purity elements using the method described in Ref. 10 (the melt-quenching technique), in 8 batches of ~ 17 g each. The outer ampoule, used as a safety precaution in Ref. 10, was not utilized so the effective cooling rate was slightly increased in this synthesis. The ampoules were annealed at 185 °C for 6 days before they were opened un-

der a nitrogen atmosphere. Half of the glassy material was ground into a rather fine powder and the rest crushed into small pieces (diam ~1 mm) and mixed with the powder. Representative pieces from the bulk were sorted out and characterized with the techniques presented in Ref. 10. It was found, as for the Ag-natural sample in Ref. 10, that the glass sample was homogeneous and exhibited no crystalline contamination, and that the oxygen contamination was of the same magnitude as before (~35 μg/g). The amount of oxygen contamination is believed to be insignificant for this system and will not affect the outcome of the experiments.

The vitreous $GeSe_2$ and $Ag_4Ge_3Se_9$ samples studied in the reflection-Raman experiments were extracted from the same materials prepared for the inelastic neutron scattering measurements. The samples were prepared by cutting slices from the bulk using a slow-speed saw with a diamond blade. They were then polished until they exhibited a smooth specular surface and mounted on microscope slides with special cement.

III. EXPERIMENTAL

A. Neutron scattering

The neutron scattering experiments were carried out at the Low-Resolution Medium Energy Chopper Spectrometer (LRMECS, see Ref. 11) at the Intense Pulsed Neutron Source at Argonne National Laboratory. The incident neutron energy E_0, and thus the incident wave vector $\mathbf{k}_0$, are selected by a rotating chopper positioned in the incoming neutron beam. The final energy E_1 and wave vector $\mathbf{k}_1$ of the scattered neutrons are derived from time-of-flight analysis of the scattering event at any given scattering angle ϕ. Neutrons are registered simultaneously in 41 detector groups (~140 detectors) covering scattering angles from 2.70° to 116.40°. The dynamic scattering function $S(Q,E)$, expressed as a function of energy transfer $E=E_0-E_1$ and momentum transfer $\mathbf{Q}=\mathbf{k}_0-\mathbf{k}_1$ for the scattering process, is, in turn, derived from the count rate in a given detector at a given time-of-flight. In the case of scattering from an isotropic material the direction of $\mathbf{Q}$ is unimportant and we may drop the vector notation.

The incident energy was fine-tuned to 60.5 meV ($\mathbf{k}_0=5.41$ Å^{-1}) as determined from the spectra in two monitors located up- and downstream of the sample position, respectively. In the case of vibrational excitations we study the neutron energy-loss side of the scattering event. The incident energy was therefore chosen around 60 meV to cover the full range of vibrational frequencies with ~5% energy resolution. The data below ~5 meV are affected by elastic scattering and would be difficult to interpret unless elaborate corrections were to be applied, and the data beyond ~45 meV suffer from a low count rate providing low statistical accuracy. We will therefore display the vibrational spectrum over only the range 5–45 meV. In the study of the structure factors data were analyzed up to $E=-10$ meV. The range in Q is approximately 0.3–9.2 Å^{-1} for elastic scattering and becomes narrower as the energy transfer E increases due to the inherent kinematic constraints that relate Q and E.

The sample material (114.87 g) was loaded into an Al foil holder (width 3 in.×height 4 in.×depth $\frac{3}{16}$ in.) which was mounted between two Cd-covered copper frames attached to the cold finger of a closed-cycle Displex refrigerator. A radiation shield surrounded the mounting assembly. The temperature, measured with a thermocouple attached to the copper frame, was maintained at $T=15\pm2$ K during all measurements. The measurements were performed in transmission geometry at 45° with respect to the incident beam. The beam size, defined by collimators, was approximately 2 in. wide and 4 in. high at the sample position.

Runs were made for the g-$Ag_4Ge_3Se_9$ sample (89 h), the empty Al holder (63 h), a Cd-plate neutron absorber (10 h), and a vanadium plate (thickness =0.1575 cm; 7 h). The transmission factor, derived from the integrated monitor counts in the two beam monitors for each run, provides a useful check of the utilized cross sections and the number of scattering units in the beam. The measured transmission factor, $T=0.692$, for the g-$Ag_4Ge_3Se_9$ sample was in agreement with calculations utilizing tabulated values for the bound scattering cross section ($\sigma_s=7.53$ b) and the absorption cross section [$\sigma_a(E_0)=14.73$ b]. It gave 0.814×10^{24} $Ag_{0.2500}Ge_{0.1875}Se_{0.5625}$ scattering units in the beam; i.e., all sample material was in the beam. We estimate that ~10% of the neutrons are scattered and ~20% are absorbed in the sample. This has important implications for the data analysis as will be seen below.

The vanadium run is used for normalization purposes. The detector efficiency factors (~50%), which are needed in order to calculate the scattering function on an absolute scale, are calculated from the vanadium spectra. The measured transmission factor $T=0.882$ for vanadium is in good agreement with calculations using 0.829×10^{24} scattering units (V atoms) in the beam, and $\sigma_s=5.20$ b and $\sigma_a(E_0)=3.28$ b for the bound scattering and absorption cross section, respectively.

The transmission factors for the sample and vanadium were used to construct composite background runs, $B_i=T_iB_E+(1-T_i)B_{Cd}$, where B_E represents the empty Al holder run, B_{Cd} the Cd run, and $i=\{$sample, vanadium$\}$. They were subtracted from the sample and vanadium runs, respectively, to obtain their corrected spectra.

B. Raman scattering

Raman scattering spectra were excited with 6471-Å krypton laser light and collected in the near 180°, backscattering geometry at room temperature. The unpolarized spectra are presented with no correction for the Boltzmann population factor. The spectra are multiplied with different scale factors to put them on a similar scale.

IV. DATA ANALYSIS

The data were analyzed using standard routines.[12] The scattering function was first reduced to a function of scattering angle and energy and was initially obtained for 39 angles, excluding two detector groups (22.20° and 31.20°) which contained noisy detectors.

Two important observations pertaining to the nuclear

properties of the elements were used to facilitate the analyses. First, the large absorption cross section for Ag makes the absorption for g-$Ag_4Ge_3Se_9$ large. We therefore omitted the multiple scattering corrections in the analysis. The multiple scattering was estimated to be $\ll 10\%$ of the primary scattering, at least for scattering angles $\phi > 45°$. The self-shielding corrections, on the other hand, are important. The data were therefore corrected for self-shielding of the primary beam due to absorption [assuming $1/\sqrt{E}$ energy dependence for $\sigma_a(E)$] and scattering processes. Second, the incoherent cross section is $<5\%$ of the total scattering cross section σ_s, and its contribution to the scattering was neglected.

The data were interpolated onto a constant-Q grid using cubic splines to obtain the scattering function in the range 0.6–8.6 $Å^{-1}$ with $\Delta Q = 0.2$ $Å^{-1}$. $S(Q,E)$ was integrated over the region of elastic scattering at constant Q to obtain the elastic structure factor $S_{el}(Q)$ and, similarly, integrated over the full energy range to obtain the total structure factor $S(Q)$. The generalized *one-phonon* vibrational density of states (GVDOS), $G(E)$, was also derived from the scattering function in a multistep process. First, using the incoherent approximation the generalized vibrational density of states was calculated. Second, the multiphonon contribution to the scattering was estimated and subtracted using an iterative procedure. Finally the GVDOS was obtained by averaging the data over an explicit Q range, here 4.40–6.80 $Å^{-1}$.

V. RESULTS

A. Elastic and total scattering

The scattering function $S(Q,E)$ (corrected for self-shielding) is shown in Fig. 1. The scattering is clearly dominated by the elastic scattering with a Q dependence that resembles the behavior of the total structure factor. The $S(Q,E)$ is also plotted in Fig. 2 with the elastic part suppressed to highlight the inelastic scattering. The introduction of Ag washes out the oscillations seen in the scattering function for g-$GeSe_2$ (Ref. 4). This, in turn, implies that the GDVOS will exhibit less pronounced peaks as discussed below.

It is interesting to compare the elastic structure factor $S_{el}(Q)$ and the total structure factor $S(Q)$ with the structure factor measured in (Ref. 10). These functions are compared in Fig. 3. $S_{el}(Q)$, obtained by integrating $S(Q,E)$ over the elastic region (-5 meV to $+5$ meV) at constant Q, measures the long-time behavior of the scattering system; i.e., the correlation between the equilibrium sites of the atoms, and will decay at large Q due to the thermal vibrations of the atoms. The total structure factor $S(Q)$, on the other hand, here obtained through integration from -10 meV to $+45$ meV, measures the correlation between the instantaneous ($t=0$) positions of the atoms and should resemble the structure factor from the diffraction experiment. $S(Q)$ in the diffraction experiment has been normalized to approach 1.0 as $Q \to \infty$.

The agreement is very good considering the coarser Q resolution in the LRMECS experiment and the different corrections applied to the data in the two cases. For instance, the incoherent scattering is included in the LRMECS results but not in the diffraction results, and multiple scattering corrections were utilized in the diffraction experiments (cylindrical geometry) whereas

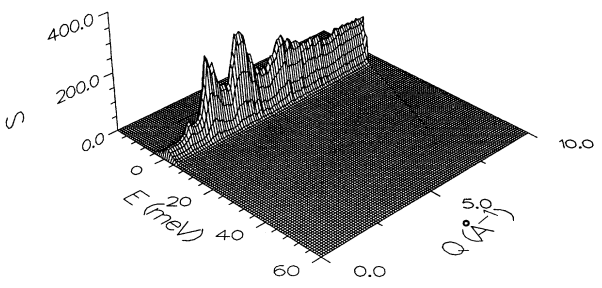

FIG. 1. Scattering function $S(Q,E)$ displayed for the entire measured (Q,E) region. Data are corrected for self-shielding effects.

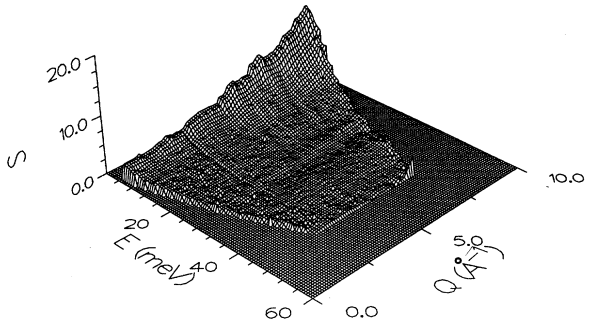

FIG. 2. Scattering function $S(Q,E)$ with the elastic scattering suppressed.

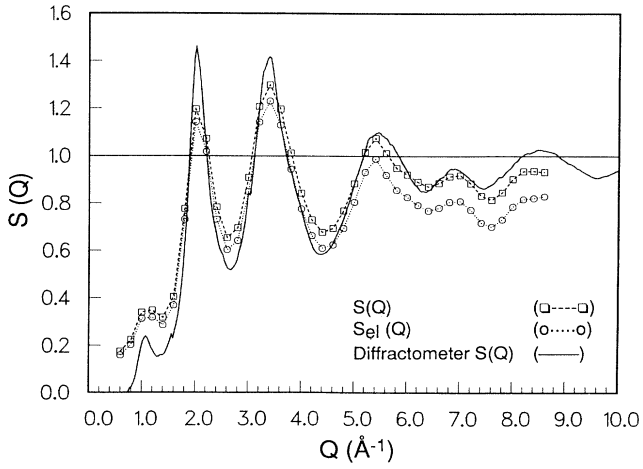

FIG. 3. Comparison of total structure factor $S(Q)$ and the elastic structure factor $S_{el}(Q)$ with the structure from the diffraction experiment. $S(Q)$ (□— — —□), $S_{el}(Q)$(0 · · · 0), diffractometer $S(Q)$ (——).

they were omitted here. This supports the validity of the assumption that the multiple scattering and incoherent scattering are not particularly important in the inelastic measurements. The fall-off in the total $S(Q)$ for $Q>7$ Å^{-1} is due to the limited energy range accessible in the integration because of the kinematic relation between Q and E. This is also true below ~ 2.8 Å^{-1}, but here inelastic scattering at large energy transfers is rather small, thus yielding a measured total $S(Q)$ which is even larger than the diffractometer $S(Q)$. However, the structure factor derived from the diffraction experiment suffers from inadequate absorption corrections and gives too low values in the small-Q region, which then explains the contradictory behavior. The less pronounced peaks and valleys in the total structure factor is due to the coarser Q resolution in this experiment.

To examine the correlations between neighboring atoms and to estimate the amplitude of the thermal vibrations we study in detail the behavior of the elastic scattering versus the total scattering.[4,11] The total $S(Q)$ can be approximated by the diffractometer $S(Q)$ which in turn can be estimated by

$$S(Q)=1.0+\sum_s C_s e^{-2W_s'}\left[\frac{\sin(QR_s)}{QR_s}\right],$$

where the summation is taken over the first few coordination shells s. C_s is the neutron-weighted coordination number as determined from the measured total distribution function $T(R)$ in Ref. 10, R_s is the position of shell s, and $2W_s'$ is the Debye-Waller exponent, here given by

$$2W_s'=\tfrac{1}{2}Q^2\langle u^2\rangle_s=\tfrac{1}{2}Q^2(\Delta_s^2+\langle u_{ii'}^2\rangle_s).$$

Δ_s^2 represents the static order of the atoms and $\langle u_{ii'}^2\rangle_s$ indicates the time-averaged difference of the vibrational displacement between atoms i and i' projected along the bond (i'—i). In the case of *uncorrelated* motions we get

$$\langle u_{ii'}^2\rangle_s=\langle u_{i\parallel}^2\rangle+\langle u_{i'\parallel}^2\rangle,$$

where $\parallel$ means projection along the bond. Furthermore, if motions are isotropic then

$$\langle u_{i\parallel}^2\rangle=\langle u_i^2\rangle/3$$

and hence

$$2W_s'=\tfrac{1}{2}Q^2(\Delta_s^2+\langle u_i^2\rangle/3+\langle u_{i'}^2\rangle/3).$$

On the other hand, completely *correlated* motions yield

$$\langle u_{ii'}^2\rangle_s=0.$$

In this case $2W_s'$ is made up of the static contribution Δ_s^2 of the mean-square displacements,

$$2W_s'=\tfrac{1}{2}Q^2(\Delta_s^2).$$

In the diffraction experiment,[10] we are unable to separate the individual components and measure only their sum

$$\langle u^2\rangle_s=\Delta_s^2+\langle u_{ii'}^2\rangle_s.$$

Table I lists the mean-square displacements $\langle u^2\rangle_s$, and the parameters C_s and R_s.

TABLE I. Fitted parameters from the diffraction experiment for g-$Ag_4Ge_3Se_9$.[a]

Shell	Correlation	Distance R_s (Å)	$\langle u^2\rangle_s^{1/2}$ (Å)	C_s
1	Ge-Se	2.371	0.056	1.730
2	Ag-Se	2.670	0.095	1.244
3	Ag-Ag[b]	2.997	0.124	0.559
4	Ag-Se[c]	3.345	0.111	0.286
5	Se-Se	3.893	0.285	10.075

[a]From Ref. 10. For the Ag-natural sample.
[b]Gaussian function was not fitted. First moment was used to calculate $\langle u^2\rangle_s^{1/2}$.
[c]Several correlations overlap in this region. Ag-Se correlation was used as a compromise.

Similarly, but with some distinct differences, we approximate the elastic structure factor by

$$S_{\rm el}(Q)=\overline{e^{-2W}}+\sum_s C_s e^{-2W_s}\left[\frac{\sin(QR_s)}{QR_s}\right]$$

with C_s and R_s having the same meaning as before and with the Debye-Waller factor given by

$$\overline{e^{-2W}}=\frac{\sum_i c_i\sigma_{s,i}e^{-Q^2\langle u_i^2\rangle/3}}{\sum_i c_i\sigma_{s,i}}=\sum_i A_i e^{-Q^2\langle u_i^2\rangle/3}.$$

The Debye-Waller factor determines the fall-off in the function at large Q. The concentrations c_i, the neutron scattering cross sections $\sigma_{s,i}$, their combined weighting A_i, and the mean-square displacement $\langle u_i^2\rangle/3$ for each element are listed in Table II. The mean-square displacements of the Ag and Se atoms were adjusted to give a reasonable fit to the experimental results (see Fig. 4), while the Ge mean-square displacement was kept unchanged from the $GeSe_2$ results (Ref. 4). Thus, we find that the amplitude of the thermal vibrations of the Ag atoms is considerably larger than those of both Ge and Se.

In the case of the elastic scattering the Debye-Waller exponent is given by

$$2W_s=\tfrac{1}{2}Q^2(\Delta_s^2+\langle u_i^2\rangle/3+\langle u_{i'}^2\rangle/3),$$

which is identical to $2W_s'$ above only in the limit of uncorrelated motions.

TABLE II. Concentrations, neutron scattering cross sections, and fitted mean-square displacements for g-$Ag_4Ge_3Se_9$.

	Ag	Ge	Se
c_i	0.2500	0.1875	0.5625
$\sigma_{s,i}$ (10^{-24} cm^2)	4.99	8.60	8.31
A_i	0.166	0.214	0.620
$\langle u_i^2\rangle/3$ (Å^2)	0.015 00	0.001 88[a]	0.000 50

[a]From Ref. 4.

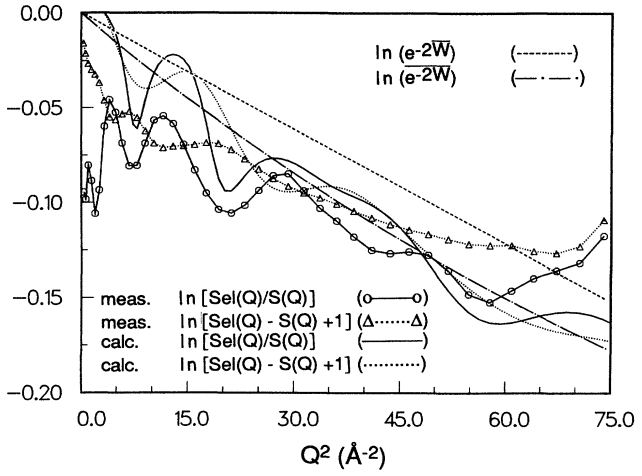

FIG. 4. Comparison of elastic scattering vs total scattering. Measured functions: $\ln[S_{el}(Q)/S(Q)]$ (0——0) and $\ln[S_{el}(Q)-S(Q)+1]$ ($\Delta\cdots\Delta$) vs calculated functions $\ln[S_{el}(Q)/S(Q)$ (——) and $\ln[S_{el}(Q)-S(Q)+1]$ ($\cdots$). Also shown in $\ln(e^{-2\overline{W}})$ with Debye-Waller coefficient $\alpha=\langle\overline{u^2}\rangle/3=0.002\,03$ Å^2(— — —) and $\ln(e^{-2\overline{W}})$ with $\langle u^2_{Ag}\rangle/3=0.015\,00$ Å^2, $\langle u^2_{Ge}\rangle/3=0.001\,88$ Å^2, and $\langle u^2_{Se}\rangle/3=0.000\,50$ Å^2 (—·—·—·).

Figure 4 displays the two quantities (measured and calculated): (i) $\ln[S_{el}(Q)/S(Q)]$ and (ii) $\ln[S_{el}(Q)-S(Q)+1]$ plotted as a function of Q^2. For comparison are also shown two functions representing the Debye-Waller factor: (iii) $\ln(e-2\overline{W})$ with $2\overline{W}=Q^2\langle\overline{u^2}\rangle/3$ and with $\langle\overline{u^2}\rangle/3=0.002\,03$ Å^2 derived from the density of states $G(E)$ and (iv) $\ln(e^{-2\overline{W}})$, with $\langle u^2_{Ag}\rangle/3=0.015\,00$ Å^2, $\langle u^2_{Ge}\rangle/3=0.001\,88$ Å^2, and $\langle u^2_{Se}\rangle/3=0.000\,50$ Å^2.

The agreement between the measured and calculated functions is satisfactory in the case of $\ln[S_{el}(Q)/S(Q)]$ but is not as good for $\ln[S_{el}(Q)-S(Q)+1]$. The ratio $\ln[S_{el}(Q)/S(Q)]$ oscillates *in phase* with $S(Q)$ which is expected. The second function, the measured $\ln[S_{el}(Q)-S(Q)+1]$, exhibits small oscillations *out of phase* with $S(Q)$ which is typical of atoms moving in phase during an acoustic mode, whereas the calculated function is phase shifted. Δ_s^2 can be estimated from the measured value of $\langle u^2\rangle_s$. We find a reasonable fit to the experimental results only if $\langle u^2_{ii'}\rangle_s\sim 0$; or $\langle u^2\rangle_s\sim\Delta_s^2$, indicating strong correlations between neighboring atoms. We note that the calculated functions are highly sensitive to the value of Δ_s^2. For example, using a 50% smaller value of Δ_s^2 forces the functions to oscillate with amplitudes out of scale (not shown) in Fig. 4. On the other hand, using a slightly larger value of Δ_s^2 ($\sim 1.05\langle u^2\rangle_s$) makes the calculated function $\ln[S_{el}(Q)-S(Q)+1]$ oscillate in phase with the measured function. Obviously, we cannot make Δ_s^2 larger than $\langle u^2\rangle_s$ since this is physically unrealistic, but it indicates that the estimated mean-square displacements are satisfactory. The discrepancy at low Q is possibly due to multiple scattering. We conclude by noting that at large Q the functions approach the mean Debye-Waller factor represented by $e-2\overline{W}$.

B. Vibrational density of states

To understand the behavior of the Ag-doped Ge-Se glass it is instructive to first review the results for pure $GeSe_2$ glass. Not surprisingly, the modeling of g-$GeSe_2$ demonstrated that the vibrational modes of an isolated tetrahedron provided a satisfactory description of the main features in both the GVDOS and the dynamic structure factor (Ref. 4). There are discrepancies, however. Experimentally Walter *et al.* find five distinct peaks and two uncertain peaks in the vibrational spectrum whereas the calculation yields only four peaks (the vibrational modes of a regular tetrahedron with point-group symmetry T_d; here denoted $\nu_1-\nu_4$). The calculated frequency ν_3 (322 cm^{-1}), for instance, is not well resolved in the experimental data and they find a split peak at lower frequencies instead. The explanation of this feature remains an open question.

The experimental GVDOS for g-$Ag_4Ge_3Se_9$ and g-$GeSe_2$ are compared in Fig. 5. Several important changes in the vibrational spectrum can readily be identified upon doping with Ag. First, the peak at $\sim$25 meV remains uniquely identified although it is shifted to a somewhat lower energy. Second, a major increase of vibrational modes below 25 meV is observed whereas there is a decrease of high energy modes around 35 meV (also shifted slightly to lower energies). Third, the increased number of low-lying modes ($5<E<10$ meV) is believed to be real but the high-energy modes beyond $\sim$40 meV are associated with large statistical errors and should accordingly be considered doubtful. Finally, rapid variations in the data, seen, for instance, around 38 meV, are within the statistical accuracy of the experiment.

At this moment it is also appropriate to compare the Raman scattering results, shown in Fig. 6, for the two

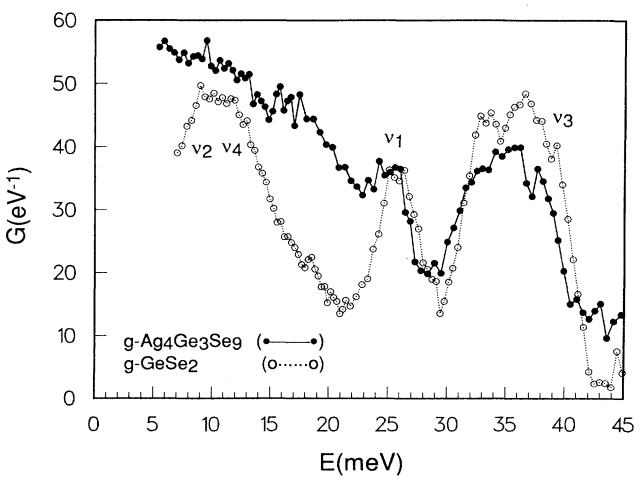

FIG. 5. Generalized one-phonon vibrational density of states, GVDOS, for g-$Ag_4Ge_3Se_9$ (●——●) and g-$GeSe_2$ (○ $\cdots$ ○). Labels $\nu_1-\nu_4$ indicate the expected frequencies of the four fundamental modes of an isolated $GeSe_{4/2}$ tetrahedron.

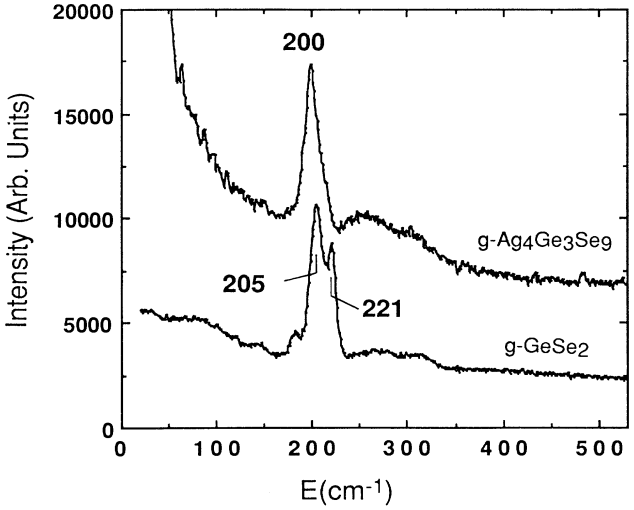

FIG. 6. Raman spectra for g-$GeSe_2$ (lower curve) and g-$Ag_4Ge_3Se_9$ (upper curve; displaced 5000 units).

glasses. First, it is interesting to note that there is an excellent agreement between our result and the result obtained by Sugai (Ref. 5) for the $GeSe_2$ glass. Second, the measured Raman spectrum for g-$Ag_4Ge_3Se_9$ shows two prominent features in relation to the undoped material: (i) The characteristic peak at 221 cm^{-1}, the so-called companion line (a manifestation of intermediate-range order), disappears upon doping with Ag. The origin of the companion line is still controversial and it has been suggested that it is due to vibrational modes of Se atoms in edge-shared bonded tetrahedra (Ref. 5) or that the in-phase motion of the dimerized Se atoms in the so-called "outrigger raft" cluster (Ref. 8) is responsible for the peak. (ii) There is a pronounced increase of intensity for energies below the main peak (200 cm^{-1}) in the Ag-doped material, qualitatively related to the increased density of low-lying modes observed in GVDOS. It is also important to note that the dominant peak at 205 cm^{-1} in g-$GeSe_2$ (although shifted slightly in energy) remains the principal peak in the entire spectrum; a feature that can be associated with the symmetric breathing mode (ν_1 mode) of a regular $GeSe_{4/2}$ tetrahedron (discussed in detail below).

C. Normal mode analysis

The main features in the frequency spectrum for an amorphous solid are determined by the local structural arrangement of the atoms. It is to be expected, therefore, that they can be reasonably well described by the characteristic vibrational modes of small, noninteracting structural elements which can be calculated using the method of normal mode analysis.[13] In such an analysis the equation-of-motion is formulated within the harmonic approximation using model parameters describing the nature of the interaction (e.g., stretch, bend, torsion) and the strength of the interaction (force constants) between the atoms. The eigenfrequencies and the corresponding eigenvectors (polarization vectors) are then derived by finding the roots of the $3N$-dimensional secular equation (N is the number of atoms in the molecule) describing the motion of the molecule. We have performed a normal mode analysis for several distinct models in an attempt to explain the origin of the vibrational modes experimentally observed in GVDOS. Ideally, the model should be able to also describe the Q dependence of the dynamic structure factor $S(Q,E)$ at selected energy excitations, which is sensitive to the structural arrangement of atoms beyond the first nearest neighbors.

Again, led by the earlier work on g-$GeSe_2$, the diffraction experiments on g-$Ag_4Ge_3Se_9$, and the Raman measurements, the vibrational properties were modeled using the $GeSe_{4/2}$ tetrahedron as the local structural element. The peaks obtained as δ functions in energy were artificially broadened using a Gaussian function (3 meV FWHM) to represent the instrumental resolution. The degeneracy of the modes is explicitly taken into account [e.g., the ν_3 mode (322 cm^{-1}) for the $GeSe_{4/2}$ tetrahedron is a triplet] and will affect the peak heights.

Initially, the GVDOS of the isolated $GeSe_{4/2}$ tetrahedron (Ge—Se bond length: 2.37 Å) was calculated. For this element, two force constants, the Ge—Se stretching constant (188 kdyn/cm and Se—Ge—Se bending constant (32 kdyn/cm), are sufficient for calculating the four fundamental modes denoted $\nu_1-\nu_4$. The ν_2 and ν_4 are the low-frequency bending modes, the ν_1 is the symmetric breathing mode, and the ν_3 is the high-frequency asymmetric stretching mode for the regular tetrahedron.

Adding Ag to the Ge-Se system makes the vibrational pattern more complex. The diffraction experiments indicate that the Ag atoms predominantly bond to Se atoms at 2.68 Å and accordingly we introduce a bond-stretching force between Ag and Se atoms. The force constant may be calculated from the second derivative of the interatomic potential with respect to the distance evaluated at the equilibrium position. Using the pair-potential from molecular dynamics calculations of Ag_2Se (Ref. 14) we get 32 kdyn/cm and from simulations of $Ag_4Ge_3Se_9$ (Ref. 15) we find 22 kdyn/cm. The experimental study of the diatomic molecule AgBr yields a value of 90 kdyn/cm and should be considered as an upper bound[16] to the force constant. Directed by these observations we ultimately found that 30 kdyn/cm was a suitable choice (discussed further below). Thus, in the modeling we add a third force to describe the interaction of Ag with the glassy network (Se) while retaining the interaction between Ge and Se but changing its strength slightly.

The most satisfactory structural element, shown in Fig. 7, consists of three $GeSe_{4/2}$ tetrahedra interconnected through four $AgSe_{3/2}$ nearly planar pyramids; three pyramids are identical whereas the fourth, in the center, is slightly different. Thus, each Ag atom is bonded to three Se atoms in an almost planar arrangement. This structural element is the end result of several logical units examined where we emphasize simplicity and where we take the nearest-neighbor distances and coordination numbers from the diffraction work.[10] The coordinates of the atoms and the derived force constants for this element are listed in Tables III and IV, respectively. Figure 8 shows the GVDOS, calculated in a normal mode

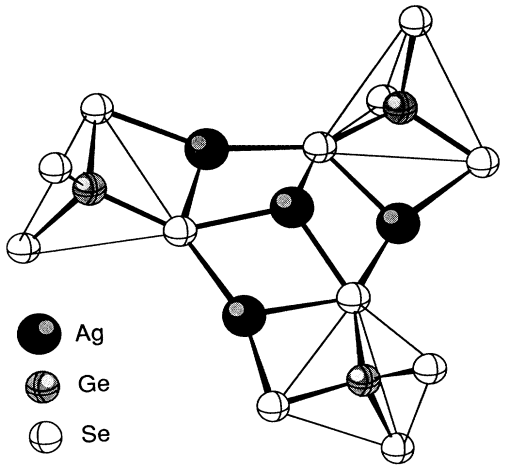

FIG. 7. Proposed $(GeSe_{4/2})_3(AgSe_{3/2})_4$ 19-atom structural element. It consists of three $GeSe_{4/2}$ tetrahedra interconnected through four Ag atoms in an almost-planar pyramidal configuration.

analysis, for both the $GeSe_{4/2}$ tetrahedron and the 19-atom element. The Ge–Se stretching constant had to be adjusted to a smaller value (170 kdyn/cm) in order to account for the fact that the ν_1 mode changed slightly in frequency. This had the important consequence of also shifting the high-frequency mode ν_3 to a lower energy, in agreement with the experiments. The analysis also correctly predicts the diminished population of the ν_3 mode. Moreover, the calculations show a substantial increase of modes with frequencies in the range 100–140 cm^{-1} arising from "pure" Ag-Se vibrations. To further explore the effect of the Ag–Se stretching constant on the spectrum, we made calculations for three different values (15, 30, and 60 kdyn/cm) of the force constant. The results are shown in Fig. 9. It is evident that a large force

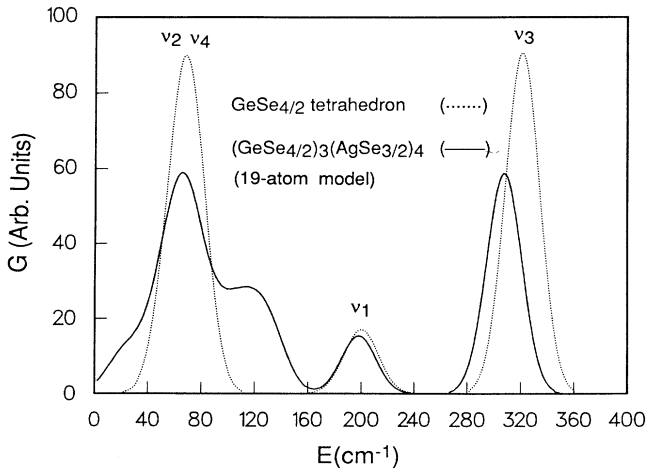

FIG. 8. Calculated GVDOS for a $GeSe_{4/2}$ tetrahedron (· · · ·) and a $(GeSe_{4/2})_3(AgSe_{3/2})_4$ structural element (——). Labels ν_1–ν_4 indicate the expected frequencies of the four fundamental modes of an isolated $GeSe_{4/2}$ tetrahedron.

TABLE III. Coordinates for the $(GeSe_{4/2})_3(AgSe_{3/2})_4$ 19-atom structural element.

Atom	X (Å)	Y (Å)	Z (Å)
Ag	+0.000	+0.000	+0.896
	+0.000	−2.800	−0.181
	+2.425	+1.400	−0.181
	−2.425	+1.400	−0.181
Ge	+1.353	+4.485	+0.000
	−4.561	−1.071	+0.000
	+3.208	−3.414	+0.000
Se	+0.000	+2.531	+0.000
	+3.646	+3.858	+0.000
	+0.884	+5.775	−1.940
	+0.884	+5.775	+1.940
	−2.192	−1.265	+0.000
	−5.164	+1.228	+0.000
	−5.443	−2.122	−1.940
	−5.443	−2.122	+1.940
	+2.192	−1.265	+0.000
	+1.518	−5.086	+0.000
	+4.559	−3.653	−1.940
	+4.559	−3.653	+1.940

constant shifts the modes (and even the ν_1 mode) to too high frequencies and that a small force constant makes them merge into the region of the low-frequency mode ν_4. Finally, we comment on the low-frequency region (below ν_2). Even in this region the analysis estimates an increase of population of modes (partly due to splitting of the degenerate low-lying modes) but it cannot fully explain the large increase observed experimentally. It should be noted that the previously published GVDOS[17] was not corrected for self-shielding effects and was averaged over a slightly different Q range which primarily caused a downward shift of the spectrum.

We also made several attempts to simplify the 19-atom structural element while still generating the main features in GVDOS. The simplest conceivable element consists of a single $GeSe_{4/2}$ tetrahedron with one Ag atom located centered above one of the sides of the tetrahedron at 2.68 Å from the Se atoms. The calculated GVDOS for this element is compared with the previous analysis in Fig. 10. It is obvious that the large model reproduces the experimental data better, but the simplified element provides better insight into the distinct modes of vibration. For example, the Ag-Se vibrational modes become more localized and appear centered at 106 cm^{-1}. The three normal modes of vibration involved are nearly degenerate in

TABLE IV. Force constants for the $(GeSe_{4/2})_3(AgSe_{3/2})_4$ 19-atom structural element.

Interaction	Type	Value (kdyn/cm)
Ge-Se	Stretch	170
Ag-Se	Stretch	30
Se-Ge-Se	Bend	32

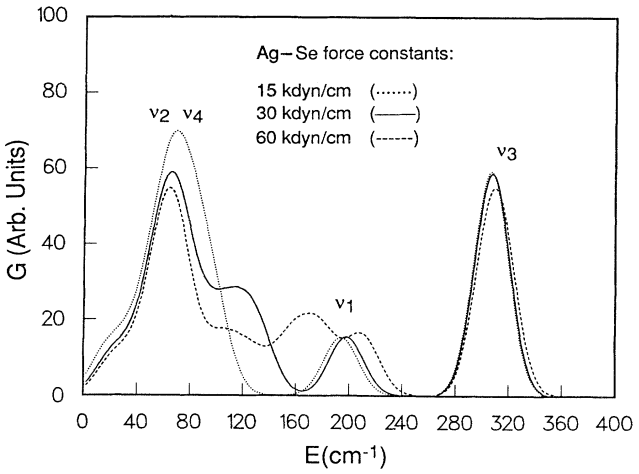

FIG. 9. Effect of the Ag–Se stretching constant on GVDOS. Force constant values: 15 kdyn/cm (· · ·), 30 kdyn/cm (——), 60 dkyn/cm (— — —).

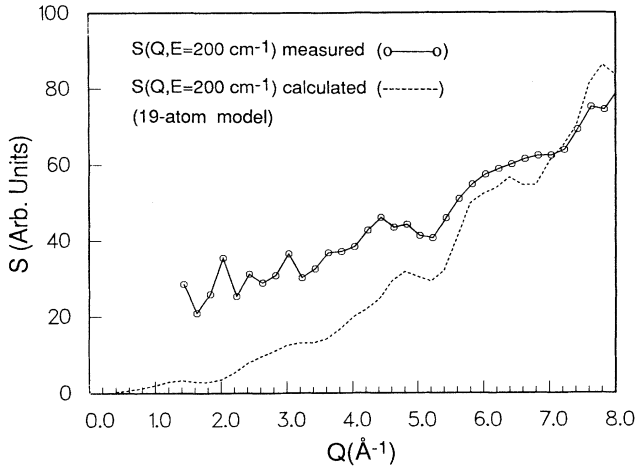

FIG. 11. Measured dynamic structure factor $S(Q,E)$ (o —— o) and calculated dynamic structure factor (— — —) for the $(GeSe_{4/2})_3(AgSe_{3/2})_4$ structural element at the ν_1 mode (200 cm^{-1}).

energy, although they show widely different displacements of the atoms. Curiously, this is the frequency one would obtain for a single fictitious Ag-Se diatomic molecule using the reduced mass and 30 kdyn/cm for the force constant in the calculation.

D. Dynamic structure factor

By studying the Q dependence of the dynamic structure factor $S(Q,E)$ at selected values of E (chosen at interesting features in GVDOS) we are able to further examine the details of the local structure of the atoms. Moreover, the normal mode analyses permit us to calculate $S(Q,E)$ for the elements explored; given the polarization vectors, it is straightforward to calculate the Q-averaged dynamic structure factor for one-phonon scattering; see Ref. 4, Eq. (8). We will concentrate the studies on the two most dominant features in the vibrational density of states (the ν_1 mode at 200 cm^{-1} and the modes around 120 cm^{-1}) in order to assess the assignment of the origin of the modes.

The experimental results and the calculated dynamic structure factor for the 19-atom element at $E = 200$ cm^{-1} are shown in Fig. 11. Obviously, the calculation reproduces quite well the oscillatory behavior seen in the experimental data. The oscillations show a period of ~ 1.8 $Å^{-1}$ reflecting correlations > 3.5 Å which is well beyond the first nearest-neighbor shells. There are some discrepancies, however, in particular in the small-Q region where the measurement shows scattered data points superimposed on a background intensity (also associated with rather large statistical errors) while the calculation exhibits a smooth behavior. This discrepancy may be due to overlapping modes contributing to the measured struc-

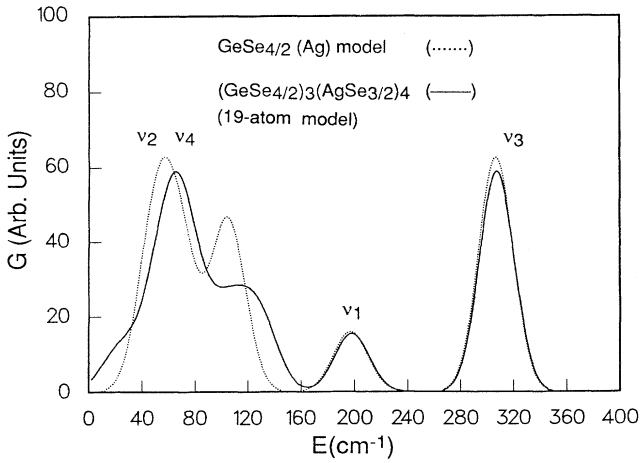

FIG. 10. Calculated GVDOS for the primitive $GeSe_{4/2}$ (Ag) element (· · ·) vs the $(GeSe_{4/2})_3(AgSe_{3/2})_4$ structural element (——).

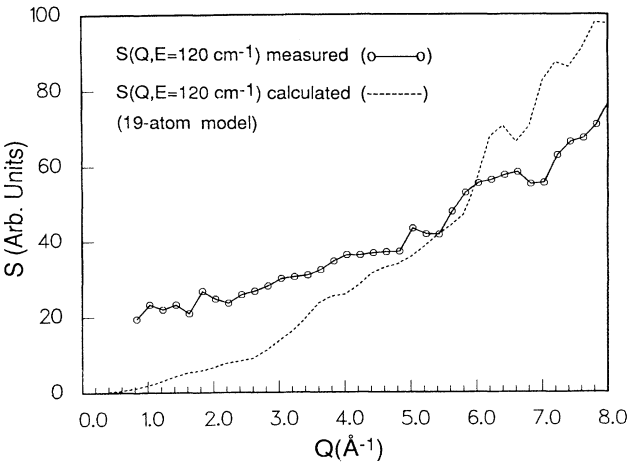

FIG. 12. Dynamic structure factors at $E = 120$ cm^{-1}. Notation same as in Fig. 11.

ture factor whereas in the calculations only single-mode vibrations are taken into account. Nevertheless, the overall agreement is quite satisfactory, thus supporting the assumption of the existence of $GeSe_{4/2}$ structural elements in the Ag-doped glass. In Fig. 12 we similarly compare the functions at $E = 120$ cm^{-1} which is at a frequency where the Ag-Se vibrational modes are likely to occur. Oscillations cannot be identified as clearly in this case, suggesting a more disordered structure. Again, we must consider the overall agreement satisfactory lending further credibility to the proposed structural element used.

VI. CONCLUSIONS

The primary conclusion of this work is that the $GeSe_{4/2}$ tetrahedron remains the basic structural element in the heavily Ag-doped Ge-Se glass. Second, the introduction of Ag destroys the intermediate-range order found in pure $GeSe_2$ glass as indicated by the disappearance of the companion line in the Raman spectrum.

Using the method of normal-mode analysis we could associate the striking increase of population of vibrational modes below the ν_1 mode at 200 cm^{-1} to complex Ag-Se vibrations with a reasonable physical value of the stretching constant. Thus, consistent with our proposed model we suggest that the Ag atoms interact with the Se atoms and break the connectivity of the covalent network. Ag-Ag interactions on the other hand seem to be of minor importance, in accordance with the fact that the glass is a fast cationic conductor. Some corner-shared tetrahedra must still exist at this composition but their intermediate-range order has been substantially reduced in agreement with our analysis based on weakly coupled $GeSe_{4/2}$ tetrahedra (through the Ag atoms) which permits the tetrahedra to vibrate virtually independent of each other.

Finally, we look forward to the results of computer simulations which, in principle, should be able to resolve some of the existing controversies. More specifically, analyses of the local structure (bond distances, bond angles, and coordination numbers) and the vibrational modes should be stressed.

ACKNOWLEDGMENTS

Dr. P. Vashishta, Dr. R. K. Kalia, and Dr. H. Iyetomi are gratefully acknowledged for stimulating discussions on molecular-dynamics simulations of glasses. Dr. J. Carpenter is also gratefully acknowledged for valuable discussions. The operations staff at the Intense Pulsed Neutron Source assisted in the neutron measurements and are gratefully acknowledged for their excellent support. The authors also wish to thank W. M. Robertson, who assisted in the Raman experiments. R. J. Dejus acknowledges the Swedish Science Research Council for its support. This work was supported by the U.S. Department of Energy, Division of Materials Sciences, Office of Basic Energy Sciences, under Contract No. W-31-109-ENG-38.

*On leave from Uppsala University, The Studsvik Neutron Research Laboratory, S-611 82 Nyköping, Sweden. Permament address: The Advanced Photon Source, Argonne National Laboratory, Argonne, IL 60439.

[1]D. L. Price, S. Susman, and A. C. Wright, J. Non-Cryst. Solids **97-98**, 167 (1987).

[2]P. H. Fuoss and A. Fisher-Colbrie, Phys. Rev. B **38**, 1875 (1988).

[3]S. Susman, K. J. Volin, D. G. Montague, and D. L. Price, J. Non-Cryst. Solids **125**, 168 (1990).

[4]U. Walter, D. L. Price, S. Susman, and K. J. Volin, Phys. Rev. B **37**, 4232 (1988).

[5]S. Sugai, Phys. Rev. B **35**, 1345 (1987).

[6]P. Vashishta, R. K. Kalia, G. A. Antonio, and I. Ebbsjö, Phys. Rev. Lett. **62**, 1651 (1989).

[7]S. C. Moss and D. L. Price, in *Physics of Disordered Materials*, edited by D. Adler, H. Fritzsche, and S. R. Ovshinsky (Plenum, New York, 1985), p. 77.

[8]J. C. Phillips, J. Non-Cryst. Solids **43**, 37 (1981).

[9]D. L. Price, S. C. Moss, R. Reijers, M. L. Saboungi, and S. Susman, J. Phys. Cond. Matter **1**, 1005 (1989).

[10]R. J. Dejus, S. Susman, K. J. Volin, D. G. Montague, and D. L. Price (unpublished).

[11]D. L. Price and J. M. Carpenter, J. Non-Cryst. Solids **92**, 153 (1987).

[12]C. K. Loong and D. L. Price (unpublished).

[13]E. B. Wilson, Jr., J. C. Decius, and P. C. Cross, *Molecular Vibrations: The Theory of Infrared and Raman Vibrational Spectra* (McGraw-Hill, New York, 1955).

[14]J. P. Rino, Y. M. M. Hornos, G. A. Antonio, I. Ebbsjö, R. K. Kalia, and P. Vashishta, J. Chem. Phys. **89**, 7542 (1988).

[15]H. Iyetomi, R. K. Kalia, and P. Vashishta (private communication).

[16]G. Herzberg, *Infrared and Raman Spectra of Polyatomic Molecules* (Van Nostrand, New York, 1945).

[17]R. J. Dejus, D. J. LePoire, D. L. Price, S. Susman, and K. J. Volin, J. Non- Cryst. Solids **114**, 37 (1989).